

RESEARCH ARTICLE

10.1002/2015JA021541

Key Points:

- An EPB event simultaneously captured from multiple locations in Indian sector
- First optical data from Indian sector suggesting MSTIDs propagation
- Simultaneous monitoring of mesospheric waves over two locations in Indian sector

Correspondence to:

A. Taori,
alok.taori@gmail.com

Citation:

Taori, A., N. Parihar, R. Ghodpage, N. Dashora, S. Sripathi, E. A. Kherani, and P. T. Patil (2015), Probing the possible trigger mechanisms of an equatorial plasma bubble event based on multistation optical data, *J. Geophys. Res. Space Physics*, 120, doi:10.1002/2015JA021541.

Received 4 JUN 2015

Accepted 14 SEP 2015

Accepted article online 18 SEP 2015

Probing the possible trigger mechanisms of an equatorial plasma bubble event based on multistation optical data

A. Taori¹, N. Parihar², R. Ghodpage³, N. Dashora¹, S. Sripathi⁴, E. A. Kherani⁵, and P. T. Patil³

¹National Atmospheric Research Laboratory, Pakala Mandal, India, ²Dr. K. S. Krishnan Geomagnetic Research Laboratory, Indian Institute of Geomagnetism, Allahabad, India, ³Medium Frequency Radar, Indian Institute of Geomagnetism, Shivaji University Campus, Kolhapur, India, ⁴Indian Institute of Geomagnetism, Navi Mumbai, India, ⁵National Institute of Space Research, São José dos Campos, Brazil

Abstract We analyze an equatorial plasma bubble (EPB) event observed in optical 630 nm image data simultaneously from Gadanki (13.5°N, 79.2°E), Kolhapur (16.8°N, 74.2°E), India. The total electron content data from Gadanki together with the ionosonde data from an equatorial Indian station, Tirunelveli (8.7°N, 77.8°E) confirmed the association of observed EPB event with equatorial spread *F* (ESF). The optical 630 nm images from a farther low-latitude Indian station Ranchi (23.3°N, 85.3°E) show clear signatures of tilted east-west wave structures propagating toward equator. Further, the upward wave energy noted in mesospheric airglow data was found to be negligible. These data suggest that possibly the off-equatorial tilted east-west structures triggered the observed EPB/ESF event.

1. Introduction

Equatorial plasma depletions/bubbles (EPB) are known to be the optical signatures of equatorial spread *F* (ESF) arising due to the irregularity processes occurring at ionospheric altitudes [Makela and Otsuka, 2011, and references therein]. The well-accepted process behind the occurrence of ESF and associated ionospheric irregularities is the generalized Rayleigh Taylor (RT) instability. For the RT instability to grow faster, a quasi-sinusoidal seed perturbation at the bottom of *F* region is required [Kelley *et al.*, 2011, and references therein]. In recent years, there had been several investigations searching these seed mechanisms. Several investigators have shown that the gravity waves of lower atmospheric origin may become a seed [e.g., Abdu *et al.*, 2009; Keskinen and Vadas, 2009; Takahashi *et al.*, 2009; Taori *et al.*, 2010, 2011a, 2011b; Tsunoda, 2010]. This mechanism is supported by the evidence that gravity waves with large amplitudes may generate polarized electric fields in the *E* region [e.g., Prakash, 1999; Varney *et al.*, 2009] which may get mapped to the *F* region from off-equatorial regions. There are also reports suggesting that large-scale wave structure may become the seed for the RT instability [e.g., Tsunoda *et al.*, 2011]. Also, Kudrki *et al.* [2007] suggested that shear flow at bottom of the *F* region may generate the shear instability which may lead to the occurrence of spread *F*. This mechanism, however, cannot account for the large-scale features and periodic spacings noted in most of the EPB observations, leaving the issues related to the seeding and occurrences under debate.

In this regard, there has been growing interest in finding the seeding mechanisms of RT instability from the traveling ionospheric disturbances, which are of midlatitude origin [e.g., Miller *et al.*, 2009]. These nighttime medium-scale traveling ionospheric disturbances (MSTIDs) have horizontal wavelengths a few hundred kilometers and are frequently observed at middle- and low-latitudes [e.g., Hunsucker, 1982; Kelley, 2011]. The nighttime MSTIDs in the northern hemisphere mainly have northwest-southeast (NW–SE) phase surfaces and propagate southwestward in the Asian, American, and European sectors [e.g., Fukushima *et al.*, 2012; Martinis *et al.*, 2010; Shiokawa *et al.*, 2006; Valladares *et al.*, 2009; Duly *et al.*, 2013]. Few investigators have suggested that MSTIDs may cause the variations in the *F* layer height [Helmboldt *et al.*, 2012; Otsuka *et al.*, 2012] and also that their quasi-sinusoidal nature may provide the required seed to the RT instability [e.g., Krall *et al.*, 2011]. In this respect, there is no report from the Indian sector which provides an optical detection of MSTIDs and their association with the occurrence of EPBs. In this study, coordinated image observations of O (¹D) 630 nm night airglow on 19–20 March 2012 from three different stations, providing coverage of the EPBs from 10°N to 32°N geographic latitude, have been used to investigate the possible connection between MSTIDs and the occurrence of EPBs. The first few images from these locations show characteristics of propagating

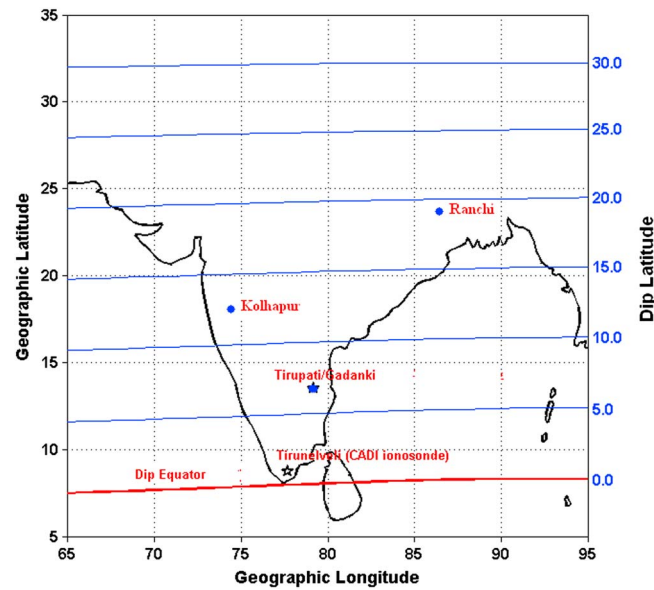


Figure 1. Map showing the locations of the stations where the observations were made for the present investigation.

MSTIDs toward the equator. After few minutes, two of the three locations exhibit the EPB structures including deep depletions in total electron content (TEC) in different longitude sectors, making the present observations novel and first set of measurements from India.

2. Experiments

2.1. Airglow Measurements

The location of the sites from where the observations for the present investigations are made is shown in Figure 1.

The airglow measurements over Gadanki (13.5°N, 79.2°E) are carried out using an imager with 90° full field of view named as NARL all-sky imager (NAI) and a narrow field photometer named mesosphere lower thermosphere photometer (MLTP).

The NARL airglow imager (NAI) located at Gadanki (13.5°N, 79.2°E) has four interference filter positions with one of them operated at 630 nm with 2 nm bandwidth and has $f/4$ optics. NAI uses a full frame CCD which has 1024×1024 pixels. These images are binned for 2×2 pixels on the chip to enhance the signal-to-noise ratio resulting in a 512×512 superpixel image. The imager is operated with a full field of view 90° which results in a spatial coverage of ~ 500 km (i.e., $>3^\circ$ in latitude and longitude). The north-south alignment of the imager has been performed using a magnetic compass. Detailed specifications of NAI and the first results are discussed by Taori *et al.* [2013].

The mesospheric temperatures are estimated using the measurements made by the Mesosphere Lower Thermosphere Photometer (MLTP) located at Gadanki (13.5°N, 79.2°E). The MLTP has $f/2$ optics and full field of view $\sim 4^\circ$. It measures mesospheric OH (at 840 and 846 nm rotational lines) and O₂ (at 866 and 868 nm rotational lines) emissions together with background emission at 858 nm with the help of temperature controlled interference filters having full width at half maximum (FWHM) ~ 0.45 nm. The MLTP uses Hamamatsu H7421-50 photon counting module as a detector. The filter movement is synchronized with the counting unit C8855 of photomultiplier tube for the operations. The temperatures are derived at OH emissions using ratio method and O₂ emissions using the slope methods described by Meriwether [1984]. More details of MLTP are described by Taori *et al.* [2011a].

The ground-based imaging observation of O (¹D) 630 nm emission from Ranchi (23.3°N, 85.3°E) and Kolhapur (16.8°N, 74.2°E) are carried out using an all-sky imaging system (developed by Keo Scientific Ltd., Canada). These imagers use $f/4$ optics and are equipped with a six-position filter wheel. The interference filters corresponding to O (¹D) 630 nm emission have a 2 nm bandwidth (full width at half maxima-FWHM). The sensors are a back illuminated thermoelectrically cooled CCDs with 512×512 pixels (over Ranchi) and 1024×1024 (over Kolhapur) with high quantum efficiency ($>90\%$) in the visible region. The exposure time used for the present measurements is 60 s (for O (¹D) 630 nm emission) at an interval of 6 min, at both locations. On the night of 19 March 2012, clear-sky conditions existed and good image data were collected for more than 10 h. At an altitude of OI 630 nm emission peak (~ 250 km), the spatial coverage of this all-sky imaging systems at 75° off-zenith angle was ~ 700 km (i.e., $>6^\circ$ in latitude and longitude). Detailed specifications of these imagers are discussed elsewhere [Narayanan *et al.*, 2009; Mukherjee *et al.*, 2010]. In the absence of photometric measurements of mesospheric temperatures, we have used zenith intensity data of OH and O (¹S) emissions to estimate the amplitude of mesospheric waves, in the present study.

In the present investigation, we do the scale analysis of the structures noted in the O (¹D) 630 nm airglow images assuming the peak emission altitude to be ~ 250 km. Further, to investigate the time evolution

characteristics, we calculate the zenith intensities using an overhead 5×5 pixel grid. Over the Indian region, March and April are the months when good sky conditions prevail during which the present campaign was conducted with airglow imagers operational from these three stations. We could collect only six clear nights of coincident observations, of which, 19–20 March 2012 was an interesting one characterized as a geomagnetically quiet ($A_p = 10$) night, making the base for the present report.

2.2. Ionospheric Measurements

The ionosonde at Tirunelveli (8.7°N, 77.8°E) is a vertical incidence Canadian Advanced Digital Ionosonde (CADI). It sweeps the radio frequency from 1 MHz to 30 MHz with a height resolution of 6 km. For the present investigation, CADI was operated at 10 min temporal resolutions. As the ionosonde is located at the dip equator, it provides the background ionospheric conditions and complimentary data on the occurrence of equatorial spread F .

2.3. Total Electron Content Measurements

A GSV4004B GPS (global positioning system) receiver has been operational over Gadanki since October 2008. The receiver uses wide bandwidth tracking loops and an internal, phase stable, ovenized crystal oscillator to compare the phase with the actual carrier phase GPS observations. Thus, it provides true amplitude, single-frequency carrier phase measurements and line of sight code and carrier phase delays on L1 (1575.42 MHz) and L2 (1227.6 MHz) from up to 11 GPS satellites in view, simultaneously and provides outputs in 22 receiver channels. The raw binary data are recorded in the computer, and total electron content (TEC) has been estimated using software which reads the Receiver Independent Exchange Format formatted raw data and processes the data for cycle slip correction, phase leveling and differential biases. Further details are discussed elsewhere [Dashora *et al.*, 2012].

3. Results and Discussion

3.1. Ionosonde Measurements Over the Equator

The ionospheric measurements corresponding to 19–20 March 2012 are summarized in Figure 2. Figure 2a plots the virtual height of the F region base ($h'F$) and frequency of F region (f_oF_2) from 1230 UT to 2030 UT. The bottom axis show the Indian Standard Time "IST" while the top axis show the Universal Time "UT" (where, $IST = UT + 5.5$). After 1230 UT, the base height of F region starts increasing from ~ 230 km and reaches to ~ 375 km before 1430 UT while, the f_oF_2 show a decreasing trend during this time. After 1430 UT, the ionosonde data showed the occurrence of ESF throughout the night. It is visible that $h'F$ and f_oF_2 during 1230–1400 UT show the presence of oscillatory features. To amplify the short period features, we remove the fourth-order polynomial fitted data (shown in Figure 2b) and obtain the residuals (Figure 2c) for $h'F$ variations. The sinusoidal waveform fit to the residuals show the presence of ~ 26 min periodicity. Similarly, the f_oF_2 data (shown in Figures 2d and 2e) show the oscillatory feature with ~ 28 min periodicity. Such oscillations are indicative of wave-like feature in the data which may either be of lower atmospheric origin, locally generated waves or the traveling ionospheric disturbances which are discussed in section 3.4.

3.2. Variation of O (1D) 630 nm Airglow Intensity During the EPB Event

3.2.1. EPB Signatures in Optical Data

A sequence of sample images indicating the occurrence of EPBs over Gadanki (13.5°N, 79.2°E) is shown in Figure 3. The left and right sides of each image show the west and east direction while the top and bottom sides indicate north and south. Each image show 500 km distance in x and y direction with location of measurement at the center. The time (in UT) of measurement is shown in the topside of each image. It is clear that deep bite outs are aligned in north-south direction, and as the time progressed these structures move eastward. Such EPB structures were noted throughout the night. To emphasis this, we calculated the average intensity over Gadanki by selecting the center of the image in a 5×5 pixel grid (which corresponds to square footprint of approximately $10 \text{ km} \times 10 \text{ km}$ at ~ 250 km altitudes). Results of this are shown in Figure 4. It is noteworthy that starting of the observation show some oscillatory features which dominated till 1600 UT. It is important to note that the total noise (including dark and readout noise) arising in the image data is less than 30. The oscillations noted show the intensity swing of 300–800 counts and also that data points are more than the required by the Nyquist criteria. Therefore, we believe these oscillations to be significant. We can see that during 1430–1600 UT there are four full cycles of oscillations which would result in a period

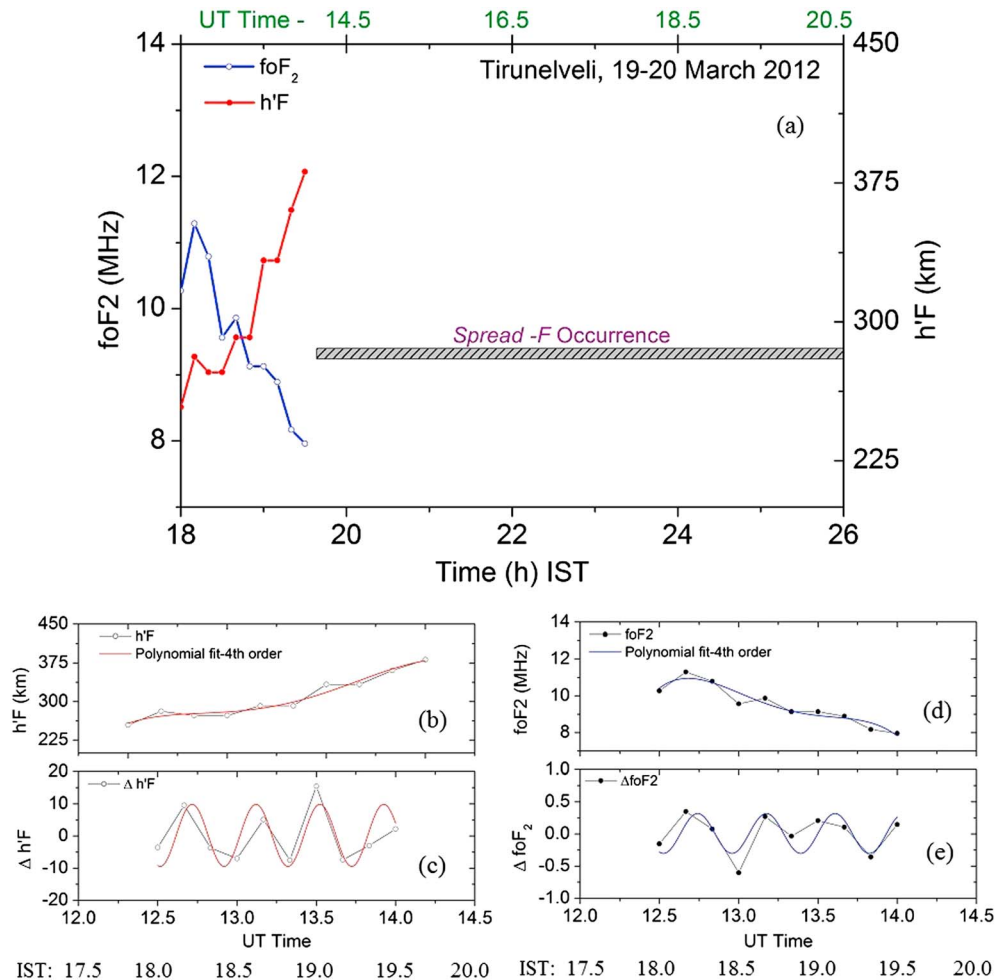


Figure 2. (a) The summary of ionospheric measurements over Tirunelveli on 19–20 March 2012 where the bottom and the top axis show the IST and UT time, respectively. The left axis represents the critical frequency of F region, while the right axis denotes the base height of F region. The time of spread F occurrence is shown as horizontal dashed area. The long and short period features in (b, c) $h'F$ and (d, e) f_oF_2 data.

of ~23 min. The ionosonde data showed the occurrence of ESF from this time onward which are also noticed in airglow data as large bite outs. Major bite outs were recorded in the 630 nm data during 1700 UT (2230 IST)–2100 UT (0230 IST). To further investigate whether the EPB event was observed at farther latitudes, we use the image measurements made from Kolhapur (16.8°N, 74.2°E). We note somewhat similar EPB structures as noted in the Gadanki data. Sample images (corresponding to the duration shown in Figure 3) emphasizing the somewhat similar EPB features are shown in Figure 5. At a farther latitude station, Ranchi (23.3°N, 85.3°E) we did not note the occurrence of EPB.

Overall, Gadanki and Kolhapur data show sharp fluctuations and bite outs in the $O(^1D)$ 630 nm night airglow intensity data. In past several reports from Indian sector have shown a close association of such bite outs with the EPBs/ESF events [e.g., Mukherjee, 2003; Sekar et al., 2008; Taori et al., 2011a]. Therefore, these signatures signify the occurrence of EPBs.

3.2.2. EPB Characteristics

As elaborated in earlier section, the optical data from Gadanki as well as Kolhapur exhibited the structures of depleted 630.0 nm intensities. It is noteworthy from the images that these structures noted as the depleted intensities, drifted toward the East as the time progressed. By cross correlating the successive images, we can calculate the drift velocity of these structures. The distances between the two depletion structures can be estimated by comparing the two minima of structures in a particular image. Please note that in this criteria we can estimate the inter depletion distances only when such structures are noted in single image. Hence,

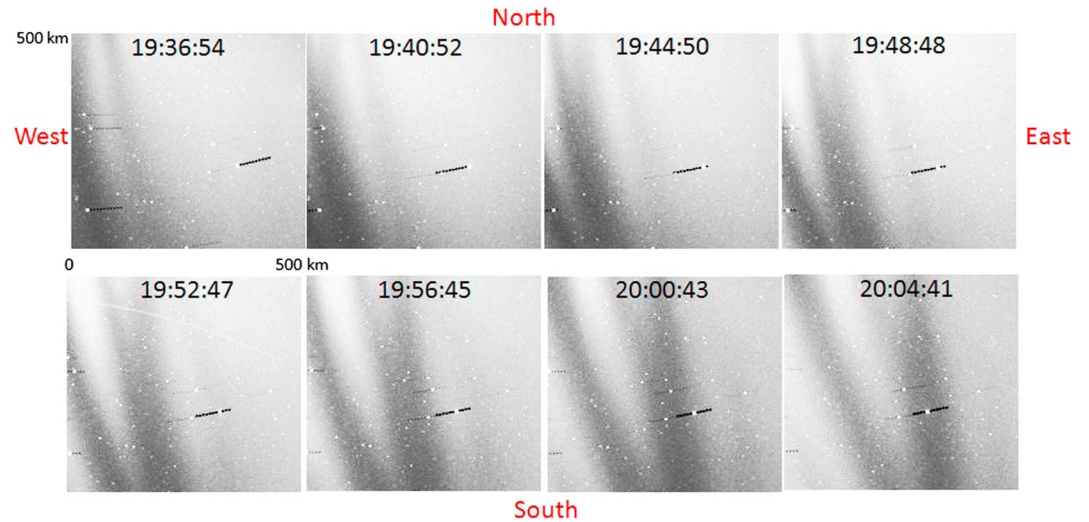


Figure 3. A sequence of images corresponding to 630 nm night airglow measurements over Gadanki on 19–20 March 2012. Depleted regions of airglow intensity with north-south aligned structures are noteworthy.

when such a separation is more than 400 km, we cannot estimate the interdepletion distances. The process followed to estimate the drift velocity in the Gadanki and Kolhapur image data has been elaborated by *Taori and Sindhya* [2014]. Figure 6 plots the estimated drift velocities over Gadanki (filled orange squares) and Kolhapur (half filled magenta color circles). The drift velocities shown are averaged for 30 min with standard deviations exhibiting the variability. We note that drift velocities from 1500 UT to 1600 UT increased to ~175 m/s and then decreased to about 45 m/s by 1930 UT. During the night observations, the interdepletion distances over Gadanki were found to be primarily ~60, 106, 180 km while, that at Kolhapur were ~70 km, 175 km, and 210 km. A detailed study on the EPB characteristics observed during March 2012 in Gadanki and Kolhapur data were reported by *Ghodpage et al.* [2014].

3.3. Total Electron Content Measurements

The occurrence of plasma bubble can be noted in GPS-TEC data as well. Figure 7a shows Vertical Total Electron Content (VTEC) as obtained for GPS satellites PRN 04 (red), PRN 17 (blue), PRN 26 (magenta), and PRN 28 (green) from 1500 UT to about 2100 UT. VTEC from PRNs 17 and 28 shows continuous rise from respective beginning until ~1600 UT. The depletions in VTEC are defined as sudden reduction in VTEC from smoothly varying levels followed by a recovery [e.g., *Dashora and Pandey*, 2005]. While PRN 17 and PRN 28

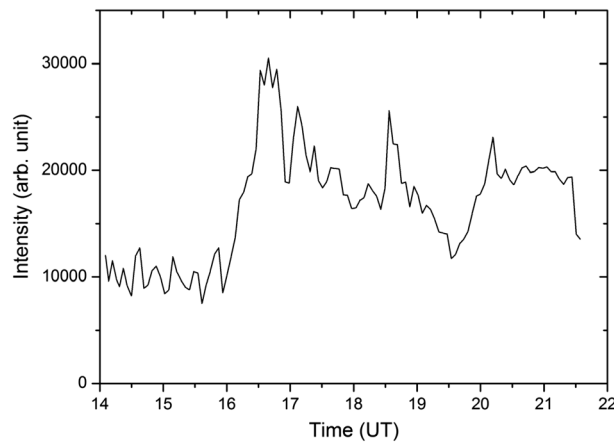


Figure 4. The 630 nm intensity variations noted over Gadanki (zenith 5×5 pixel average). It is evident that data show large fluctuations indicating the occurrence of EPBs.

reveal such depletions starting from 1600 UT and ending at 1730 UT and 1900 UT, respectively, other two satellites PRN 04 and PRN 26 show multiple sharp reductions in VTEC resembling depletions at ~1700 UT and continue to exhibit such structures until 2000 UT (postmidnight). The depth of depletions can be noted from the successive fall and recovery values of VTEC. It shall be noted that different PRNs show observations of depletions at different times and at different depths. The effect of line of sight geometry of moving GPS satellites vis-à-vis the GPS receiver at ground causes such differences and was explained by *Dashora et al.* [2012] in detail. The spatiotemporal variations

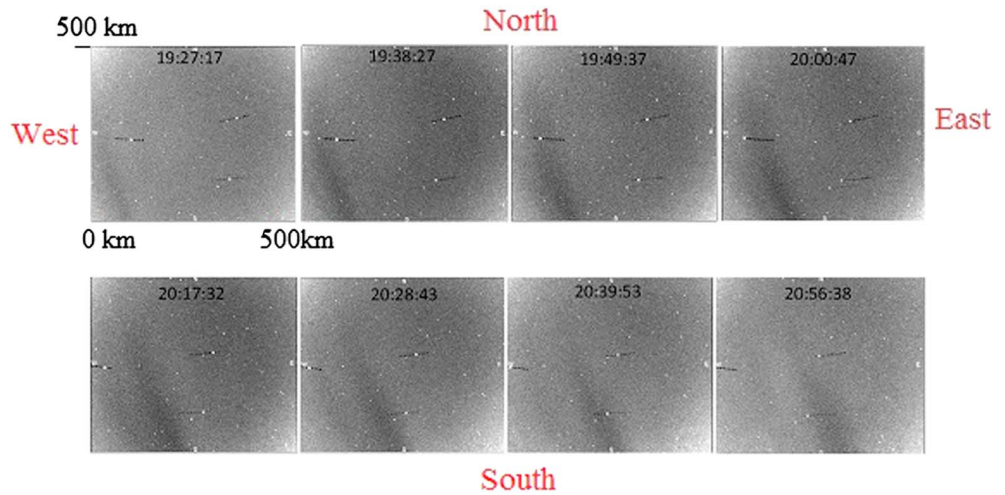


Figure 5. A sequence of images corresponding to 630 nm night airglow measurements over Kolhapur on 19–20 March 2012. Depleted regions of airglow intensity with north-south aligned structures are noteworthy.

of VTEC during depletions are shown in Figure 7b through a map of ionospheric pierce points (IPPs) corresponding to aforementioned PRNs as seen from Gadanki (13.5°N, 79.2°E). The depletions given in the time series plot of Figure 7a can be envisaged to be occurring through the respective line of sight of moving GPS satellites assuming a height of IPP to be 300 km in this case. The respective time in UT has been annotated over the curves. Large depletions that occurred for PRN 17 and PRN 28 are obviously discernible from the color-coded VTEC fluctuations. For PRN 17, the depletions that occurred before 1800 UT are seen for a range of latitudes from 12 to 15°N along about 77°E longitude while that for PRN 28, depletions are seen along latitude of ~15°N corresponding to a small range of longitude (76–77°E). Uniquely placed among the given set of PRNs, PRN 26 passed from north to south and remained almost along 74°E longitude albeit at lower elevation angles, remained westward from Gadanki and could capture the depletions due to another sets of EPBs between 1700 UT and 2000 UT. The PRN 04 passed from south to north and after showing broad minima around 1700 UT, it passed almost overhead Gadanki at about 1910 UT capturing depletions again. To summarize, the GPS-VTEC observation presented in Figures 7a and 7b show large depletions in TEC confirming the presence of EPBs on 19–20 March 2012 in Indian region as stated in section 3.2.

3.4. Probable Cause of the EPB Event

In general, RT instability is well-accepted process behind the occurrence of ESF/EPBs. For a fast growth of RT instability, a seed of quasi-sinusoidal nature has been often hypothesized [e.g., Kelley, 1989]. In this section we

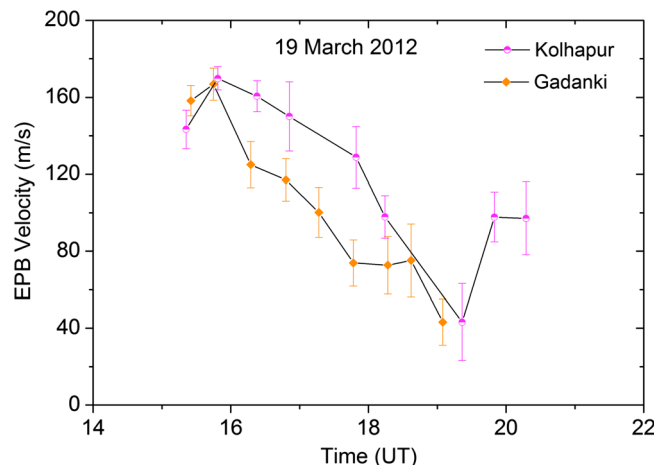


Figure 6. The variation of EPB drift velocity over Gadanki and Kolhapur on 19 March 2012.

try to identify the seed which is most tenable on this night.

In this regard, as far as the seeding of EPB is concerned, role of upward propagating waves are shown to have association by several investigations worldwide [e.g., Fritts et al., 2008; Takahashi et al., 2009; Taori et al., 2011a, 2011b, 2013]. These investigators have shown close correspondences between mesospheric gravity waves and EPB occurrences. Interestingly, from Gadanki measurements, on 17–18 March 2012 (which is just 1 day earlier than the case presented in this report), Taori et al. [2013] showed the occurrence of EPBs with periodic spacing in

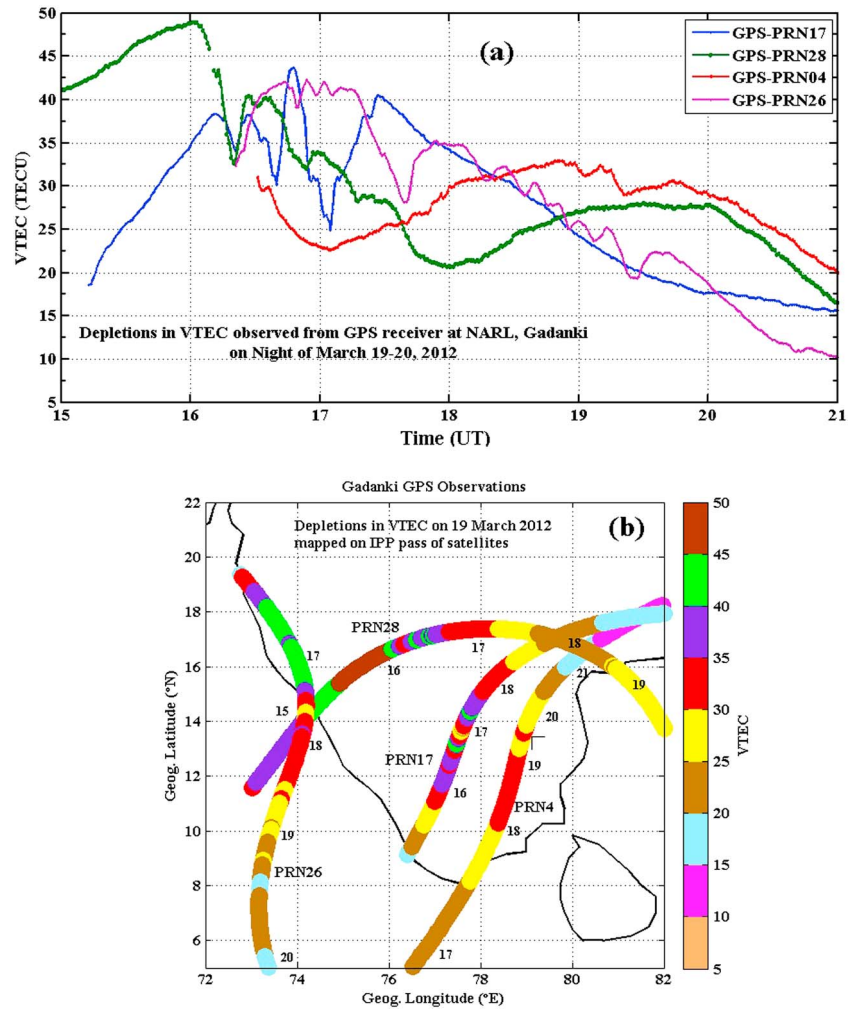


Figure 7. (a) GPS-total electron content measurements made from Gadanki exhibits the deep bite outs in TEC and high variability caused by the EPB dynamics. (b) Large longitudinal and latitudinal variability in EPB is noteworthy, where the time evolution is shown in the PRN track itself.

the EPB structures having a close correspondence with the wavelengths noted in the upper mesospheric waves. Apart from these investigations over Indian sector, there had been reports suggesting a correlation between the horizontal wavelengths monitored in the OH emission data and the interdepletion distances measured in $O(^1D)$ emission data [e.g., Paulino et al., 2011]. The imager data from Gadanki as well as Kolhapur do not reveal any wave event at OH as well as $O(^1S)$ data which represent ~ 87 and 97 km altitudes. To further rule out this possibility, the narrowband photometers data over Gadanki, which have better sensitivity for small amplitude waves, is scrutinized (Figure 8). Figures 8a and 8b show the temperature data with fitted (sinusoidal) principal wave in the nocturnal variations while Figures 8c and 8d show the residual wave present in the data. We note that 0.9 h (~ 50 min) wave is present in both data which show downward phase propagation. The delay estimated through the cross correlation analysis is ~ 20 min which results in vertical phase velocity of 5.8 m/s, indicating the vertical wavelength of wave to be ~ 18 km. However, important to note is that the amplitude of this wave at OH and O_2 emission altitude is ~ 7 K and 5 K, respectively. In general, upon its upward propagation, wave shall grow in amplitude to conserve its energy [e.g., Fritts and Alexander, 2003]; hence, this suggests that wave energy is lost in the medium making them a weak candidate for EPB seed mechanism [e.g., Taori et al., 2010]. Apart from this, other short-period waves are also present in the data; however, Lomb-Scargle periodogram analysis reveal that most of the waves had smaller amplitudes at O_2 altitudes compared to the OH altitudes, indicating insignificant wave forcing from equatorial Indian sector.

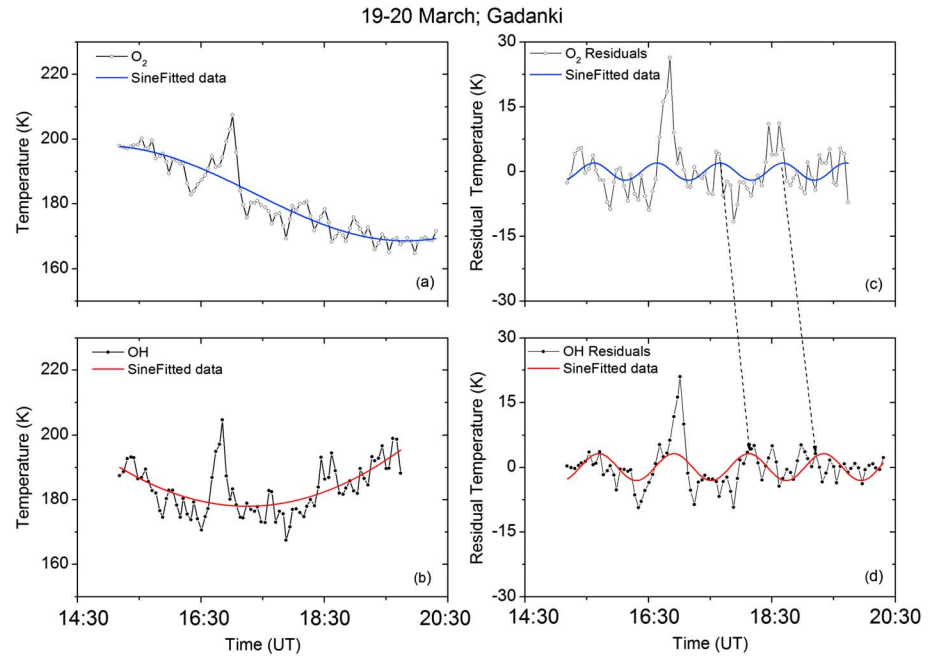


Figure 8. Upper mesospheric OH (open circles with black connecting lines) and O₂ temperature variations noted on 19–20 March 2012 over Gadanki. (a, b) The temperature data together with principal wave fit. (c, d) The corresponding residuals with best fitted sinusoidal waves. Presence of short-period oscillations in residual data and the downward phase propagation is shown as arrow lines.

As the seeding may happen from a farther location as well, similar analysis was performed for the mesospheric data collected over Kolhapur. The mesospheric OH and O (¹S) intensity data observed over Kolhapur is plotted in Figure 9. It is noted that the nocturnal variability is dominated by a wave having period ~9 h (Figures 9a and 9b). The residuals show the amplitudes of shorter waves at OH emission altitude to be ~2% while at O (¹S) the amplitudes are <1%. We believe that it is an indication that at ~97 km, the upward propagating gravity wave amplitudes were insignificant and hence their role to seed the EPB event is not defensible.

The seeding for the RT instability can be of middle- or high-latitude origin which is known as traveling atmospheric disturbances. To seek the possibility of this, we look into the 630.0 nm O(¹D) data collected over Ranchi (Figure 10). The image covers about 1500 km diameter at the peak 630.0 nm airglow altitudes. It is interesting to note that in the start of the observations, i.e., at 1502 UT (2030 IST), data from Ranchi show a band-type structure appearing in northeast corner of the image. This structure is indicated with red line mark in the image while the propagation direction is shown as green arrows. The Ranchi data at 1517 UT show another band-type structure to appear in the image. Using the cross correlation between these structures in successive images, we estimate the pixel displacements in x-y direction by which we estimate the horizontal wavelength, propagation direction, and phase velocity of the structure. The approximate horizontal wavelength of this structure is calculated to be ~185 km. These structures had an average phase velocity of ~140 ± 30 m/s at an angle of 43° from the east (the structures are indicated by red lines, while the movement is indicated by green arrows). This suggests a time period of the moving structure to be ~22 min. The line plot of this structure revealed peak-to-peak perturbation amplitude to be ~15–20%. The characteristics of this moving structure, in particular the propagation angle and velocity match well with the characteristics of MSTIDs [e.g., Garcia et al., 2000; Shiohawa et al., 2009; Makela et al., 2010]. It is important to know whether some signatures of same type were observed over Kolhapur and Gadanki so that equatorward propagation of these structures can be supported. As the image contrast during early hours at Kolhapur and Gadanki is not sufficient to note these structures, we look into the zenith intensity plot shown in Figure 4. It is evident that oscillations of similar periods were noteworthy at both these location with somewhat pronounced signatures in Gadanki data during 1400–1600 UT.

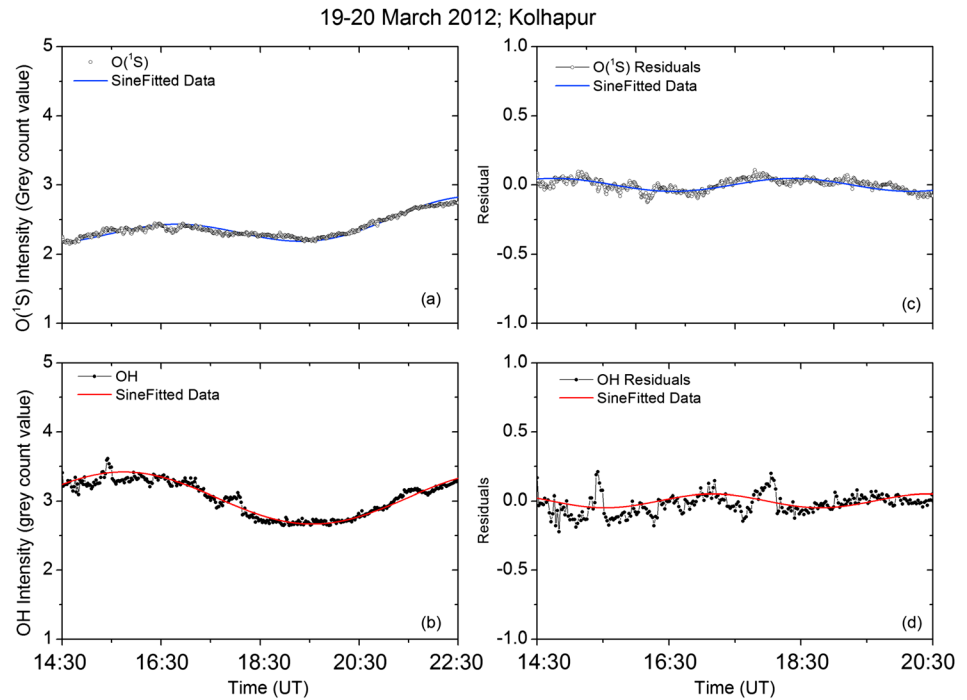


Figure 9. (a, b) The mesospheric OH and O(¹S) intensity data over Kolhapur together with the best fitted wave. (c, d) The corresponding residual data are shown with best fitted sinusoidal wave.

To further support and understand the nature of forcing, we focus on the ionospheric data from equatorial station Tirunelveli, where the EPBs are generated. In Figure 11, we present the reanalysis of digisonde observations from Tirunelveli. The temporal variation of heights corresponding to 5–8 MHz are plotted in Figure 11a as solid curves. The dashed curves represent the best polynomial fits. Figure 11b plots the height fluctuation ($\Delta h = h - h_{fit}$) are plotted for these frequencies. The cross-correlation distribution of these fluctuations is presented in Figure 11c. The cross correlation is defined as follows:

$$\eta(h, t) = \frac{\sum_5^8 \Delta h(f_1, t) \Delta h(f_2, t)}{h(f_1, t)_{max}} ; 5 \leq f_1 \leq 8 \text{ MHz}; 5 \leq f_2 \leq 8 \text{ MHz}$$

In the above, η is the cross-correlation coefficient and h_{max} is used to shift the curves for different frequencies. We note the following features from Figure 11c. The cross correlation before and after 14:54 UT (a dashed vertical line is drawn at 14:54 UT in Figures 11a and 11b) are different such that the isocorrelation contours before this time has downward propagation with time while after this time, they remain standing. Moreover, the correlation before and after this time are weaker and stronger, respectively. The downward propagation is the manifestation of the gravity waves as known from previous studies [Abdu *et al.*, 2009]. The disappearance of the downward propagation is an indication of the development of EPB often noticed from previous studies [Abdu *et al.*, 2009]. This disappearance is accompanied by the intensification of cross correlation that suggests the involvement of highly correlated dynamics such as instability dynamics.

Therefore, it can be said that over Tirunelveli, the wave-like features and EPB are present before and after 14:54 UT. This time coincides with the time of appearance of MSTIDs over Ranchi, i.e., EPBs over equator and MSTIDs over low latitude occur almost simultaneously. The presence of EPB at Gadanki was noted after 20 min from this time during which the EPB over equator has ascended to the apex height of geomagnetic line connecting 250 km altitude over Gadanki.

The simultaneous occurrence of EPB and MSTIDs is another common aspect, apart from both of them having similar wavelengths, which suggest that the common forcing is involved for their generation. In this context, the presence of MSTIDs associated wave-induced disturbances before 14:54 UT, i.e., before the occurrence of EPBs classify the MSTIDs as a possible common forcing for both of them. To further support this possibility,

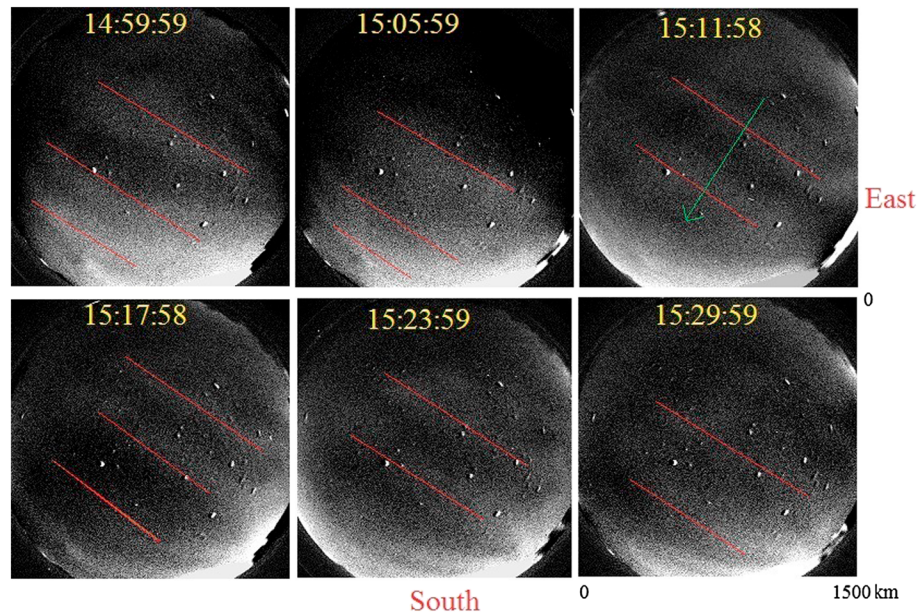


Figure 10. The 630.0 nm airglow image sequence monitored over Ranchi, exhibiting the band-type structure movement. The red lines indicate the position of wavefronts, while the green arrow shows the direction of propagation.

we may note three peaks in the cross-correlation distribution before 14:54 UT which are associated with the wave-like oscillations. These temporal structures can be equally interpreted as the spatial structures (assuming the drift velocity ~ 145 m/s and that the temporal variations are due to horizontal displacement of the features) suggesting the presence of at least three wavefronts at the equator before the occurrence of the EPBs. The presence gravity waves before EPBs/MSTIDs and MSTIDs favor that the MSTIDs propagation toward the equator was already in-place and earlier than they were observed in the optical data.

4. Summary

Our results show the occurrence of EPB event over the equatorial and low-latitude Indian sector. We note that the amplitudes of mesospheric gravity waves were very small. At the same time we noted northeast to the southwest propagating wave (MSTIDs) in the O (1D) 630 nm emission data. Optical signatures of this propagation were noted till 10° latitudes. The period of MSTIDs was about 22 min while the period of oscillatory feature noted in ionosonde was about 26–28 min which are very close. A close resemblance in these two periods suggests them to be associated with similar feature. Though, the geometry of propagating MSTIDs suggest them getting mapped to the west of the location of observations, we do not have an exact estimate on the longitudinal extent of their phase fronts. However, a similar signature was noted in the ionospheric data at Tirunelveli which is situated very close to the equator. It is possible that MSTIDs had sufficiently long-phase fronts to trigger the noted undulations in the ionosonde data. Even otherwise, a recent simulation by Krall *et al.* [2013] suggests that linear growth rate is maximum when seed field centered around 300 km is near about 10° latitudes. Therefore, we have reasons to believe that the eastward (westward) component of polarized electric fields associated with the MSTIDs in the region of low densities would result in the upward (downward) plasma drifts, transporting the *F* region plasma to higher (lower) altitudes causing the *F* layer movement as noted in the ionosonde data. It may be argued that oscillations noted in the *h'F* and f_oF_2 may be of local origin. However, most of the theories related to the local in situ generation of gravity waves at ionospheric heights rely on either secondary wave generation by the breaking of upward propagating gravity waves [e.g., Fritts and Alexander, 2003] or the solar terminator wave as explained by earlier investigators [e.g., Galushkov *et al.*, 1998; Forbes *et al.*, 2008]. Absence of any large-amplitude mesospheric waves over Gadanki and Kolhapur and lower atmospheric convective activity nearby the Gadanki location rules out the possibility of secondary wave generation. It may further be argued that secondary waves generated at far

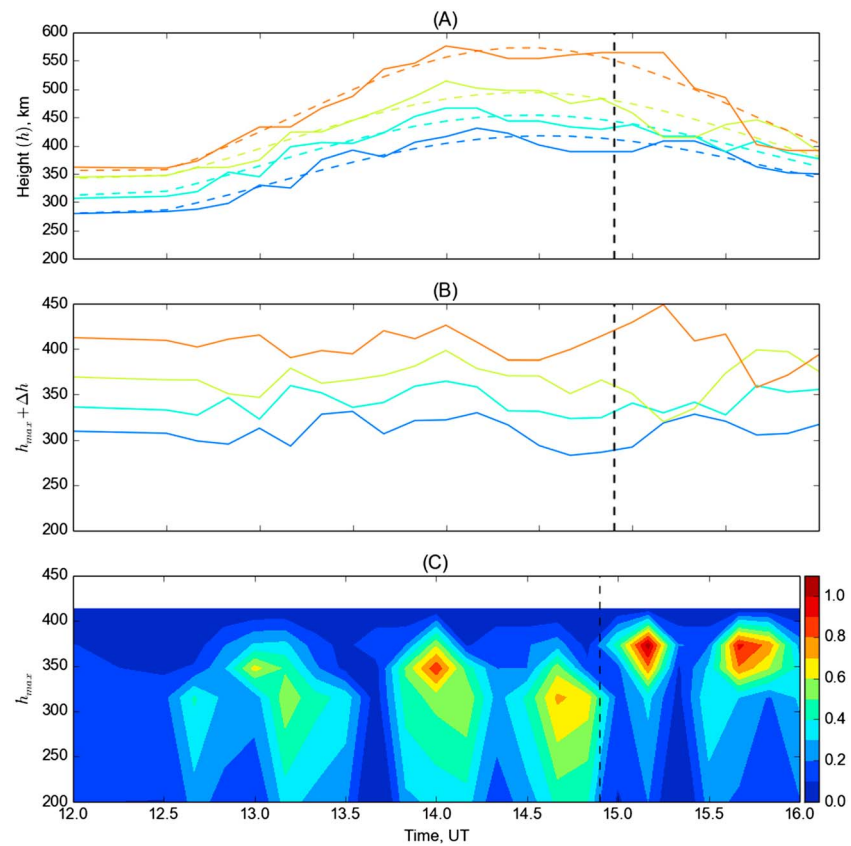


Figure 11. Digisonde data from Tirunelveli exhibiting (a) temporal variation of heights corresponding to 5–8 MHz together with dashed curves representing the polynomial fits, (b) the height fluctuation ($h - h_{fit}$), and (c) the cross-correlation distribution of the fluctuation.

places may reach the ionospheric altitudes, but absence of deep convection nearby the south Asian region suggests that if this is a possibility, then such waves have to travel almost horizontal. If this is the case, the ionospheric kinematic viscosity and molecular diffusion would lead to strong damping of such waves [e.g., *Vadas and Fritts, 2005*]. Further, as pointed out by *Forbes et al. [2008]*, the solar terminator wave period and horizontal wavelength is expected to be ~ 30 min and ~ 1000 km which is not the case in the present observations. However, these waves are expected to travel similar to that of TIDs. Further, *Balthazor and Moffett [1997]* pointed out that the TIDs can not only reach the equator but propagate across as well.

Overall, it looks reasonable to believe that a close resemblance between the observed period of wave-like feature in airglow images and the period of oscillation noted in $h'F$ and f_oF_2 may be signatures of similar features, i.e., MSTIDs. As far as the seeding of RT instability by these features are concerned, our results are in line with the theory of *Krall et al. [2011]*, where they have modeled the EPB triggering due to non-equatorial sources (MSTIDs). Their result clearly suggests that for a horizontal propagation angle $40\text{--}50^\circ$ (from the east), the e -folding time is $\sim 7\text{--}8$ min. Further, *Miller et al. [2009]* studied the EPB triggering by MSTIDs in American sector and found that it takes 10–15 min to trigger the EPB after they reach the equator. Therefore, we have a reason to believe that our results are supporting the trigger of EPB due to the MSTIDs. Unique to the present study is that so far most of the reports suggest that MSTIDs trigger the EPBs that occur near the midnight [e.g., *Miller et al., 2009*], while, we show MSTIDs possibly triggering the post evening EPBs. Added to this uniqueness is that the present observations are first from Indian sector to provide simultaneous imaging of MSTIDs and EPB together with an information on the mesospheric wave features. Our effort is to gather more information related to the mesosphere lower thermosphere processes which have relevance in improving the satellite navigation and related parameter forecasting and bring them to the notice of the community.

5. Conclusions

The present investigation based on the optical data from three stations with supporting ionospheric data from equatorial station lead to the following conclusions.

1. First image evidence of MSTIDs propagation toward the equator over Indian sector having their horizontal wavelength ~ 185 km and period of ~ 22 min.
2. Before the occurrence of ESF, the ionospheric parameters ($h'F$ and f_oF_2) show oscillatory features with periods ~ 26 min.
3. The amplitude growth of upward propagating waves at mesospheric altitude was found to be insignificant over off-equatorial latitudes.
4. The seeding of RT instability by MSTIDs is found to be the one of the probable cause behind the observed EPB event.

Acknowledgments

The present investigation is carried out under NARL-SAFAR program and is supported by the Department of Space and Department of Science and Technology, Government of India. Authors acknowledge the help of Mr. Liyakat Basha and V. Kamalakar in carrying out airglow observations over Gadanki. The data used in the present study can be obtained through dc.narl.gov.in or, by sending an email request to the corresponding author mentioning the aim and objectives.

Alan Rodger thanks Hisao Takahashi and Narayan Chapagain for their assistance in evaluating this paper.

References

- Abdu, M. A., E. A. Kherani, I. S. Batista, E. R. de Paula, D. C. Fritts, and J. H. A. Sobral (2009), Gravity wave initiation of equatorial spread F/plasma bubble irregularities based on observational data from the SpreadFEx campaign, *Ann. Geophys.*, *27*, 2607–2622, doi:10.5194/angeo-27-2607-2009.
- Balthazor, R. L., and R. J. Moffett (1997), A study of atmospheric gravity waves and travelling ionospheric disturbances at equatorial latitudes, *Ann. Geophys.*, *15*, 1048–1056.
- Dashora, N., and R. Pandey (2005), Observations in equatorial anomaly region of total electron content enhancements and depletions, *Ann. Geophys.*, *23*, 2449–2456.
- Dashora, N., A. Taori, and A. K. Patra (2012), Multi-instrument observations of winter solstice F-region irregularities during low solar activity, *Indian J. Radio Space Phys.*, *41*, 220–232.
- Duly, T. M., N. P. Chapagain, and J. J. Makela (2013), Climatology of nighttime medium-scale traveling ionospheric disturbances (MSTIDs) in the Central Pacific and South American sectors, *Ann. Geophys.*, *31*, 2229–2237, doi:10.5194/angeo-31-2229-2013.
- Forbes, J. M., S. L. Bruinsma, Y. Miyoshi, and H. Fujiwara (2008), A solar terminator wave in thermosphere neutral densities measured by the CHAMP satellite, *Geophys. Res. Lett.*, *35*, L14802, doi:10.1029/2008GL034075.
- Fritts D. C., M. J. Alexander (2003), Gravity wave dynamics and effects in the middle atmosphere, *Rev. Geophys.*, *41*(1), 1003, doi:10.1029/2001RG000106.
- Fritts, D. C., et al. (2008), Gravity wave and tidal influences on equatorial F based on observations during the Spread F Experiment (SpreadFEx), *Ann. Geophys.*, *26*, 3235–3252.
- Fukushima, D., K. Shiokawa, Y. Otsuka, and T. Ogawa (2012), Observation of equatorial nighttime medium-scale traveling ionospheric disturbances in 630-nm airglow images over 7 years, *J. Geophys. Res.*, *117*, A10324, doi:10.1029/2012JA017758.
- Galushkov, G., V. V. Paznukhov, Y. M. Yampolski, and J. C. Foster (1998), Incoherent scatter radar observations of AGW/TID events generated by the moving solar terminator, *Ann. Geophys.*, *16*, 821–827.
- Garcia, F. J., M. C. Kelley, J. J. Makela, and C.-S. Huang (2000), Airglow observations of mesoscale low-velocity traveling ionospheric disturbances at midlatitudes, *J. Geophys. Res.*, *105*(A8), 18,407–18,415, doi:10.1029/1999JA000305.
- Ghodpage, R. N., A. Taori, P. T. Patil, S. Gurubaran, S. Sripathi, S. Banola, and A. K. Sharma (2014), Simultaneous optical measurements of equatorial plasma bubble (EPB) from Kolhapur (16.81°N, 74.21°E) and Gadanki (13.51°N, 79.21°E), *J. Atmos. Sol. Terr. Phys.*, *121*, doi:10.1016/j.jastp.2014.05.008.
- Helmboldt, J. F., T. J. W. Lazio, H. T. Intema, and K. F. Dymond (2012), A new technique for spectral analysis of ionospheric TEC fluctuations observed with the Very Large Array VHF system: From QP echoes to MSTIDs, *Radio Sci.*, *47*, RS0L02, doi:10.1029/2011RS004787.
- Hunsucker, R. (1982), Atmospheric gravity waves generated in the high latitude ionosphere: A review, *Rev. Geophys.*, *20*, 293–315, doi:10.1029/RG020i002p00293.
- Kelley, M. C. (1989), *The Earth's Ionosphere, Plasma Physics and Electrodynamics*, Int. Geophys. Series, vol. 43, Academic, San Diego, Calif.
- Kelley, M. C. (2011), On the origin of mesoscale TIDs at midlatitudes, *Ann. Geophys.*, *29*, 361–366, doi:10.5194/angeo-29-361-2011.
- Kelley, M. C., J. J. Makela, O. de La Beaujardiere, and J. Retterer (2011), Convective Ionospheric storms: A review, *Rev. Geophys.*, *49*, RG2003, doi:10.1029/2012RG00034010.
- Keskinen, M. J., and S. L. Vadas (2009), Three dimensional nonlinear evolution of equatorial ionospheric bubbles with gravity wave seeding and tidal wind effects, *Geophys. Res. Lett.*, *36*, L12102, doi:10.1029/2009GL037892.
- Krall, J., J. D. Huba, S. L. Ossakow, G. Joyce, J. J. Makela, E. S. Miller, and M. C. Kelley (2011), Modeling of equatorial plasma bubbles triggered by non-equatorial traveling ionospheric disturbances, *Geophys. Res. Lett.*, *38*, L08103, doi:10.1029/2011GL046890.
- Krall, J., J. D. Huba, G. Joyce, and M. Hei (2013), Simulation of the seeding of equatorial spread F by circular gravity waves, *Geophys. Res. Lett.*, *40*, 1–5, doi:10.1029/2012GL054022.
- Kudeki, E., A. Akgiray, M. Milla, J. L. Chau, and D. L. Haysell (2007), Equatorial Spread-F initiation: Post-sunset vortex, thermospheric winds, gravity waves, *J. Atmos. Sol. Terr. Phys.*, *69*, 2416–2427.
- Makela, J. J., and Y. Otsuka (2011), Overview of nighttime ionospheric instabilities at low- and mid-latitudes: Coupling aspects resulting in structuring at the mesoscale, *Space Sci. Rev.*, *168*, 419–440, doi:10.1007/s11214-011-9816-6.
- Makela, J. J., E. S. Miller, and E. R. Talaat (2010), Nighttime medium-scale traveling ionospheric disturbances at low geomagnetic latitudes, *Geophys. Res. Lett.*, *37*, L24104, doi:10.1029/2010GL045922.
- Martinis, C., J. Baumgardner, J. Wroten, and M. Mendillo (2010), Seasonal dependence of MSTIDs obtained from 630.0 nm airglow imaging at Arecibo, *Geophys. Res. Lett.*, *37*, L11103, doi:10.1029/2010GL043569.
- Meriwether, J. W. (1984), Ground based measurements of mesospheric temperatures by optical means, in *International Council of Scientific Unions Middle Atmosphere Handbook*, vol. 13, edited by R. Vincent, pp. 1–18, Natl. Aeron. and Space Admin, Greenbelt, Md.
- Miller, E. S., J. J. Makela, and M. C. Kelley (2009), Seeding of equatorial plasma depletions by polarization electric fields from middle latitudes: Experimental evidence, *Geophys. Res. Lett.*, *36*, L18105, doi:10.1029/2009GL039695.

- Mukherjee, G. K. (2003), Studies of equatorial F-region depletions and dynamics using multiple wavelength nightglow imaging, *J. Atmos. Sol. Terr. Phys.*, *65*, 379–390.
- Mukherjee, G. K., R. Pragati Shikha, N. Parihar, R. Ghodpage, and P. T. Patil (2010), Studies of the wind filtering effect of gravity waves observed at Allahabad (25.45°N, 81.85°E), *Earth Planets Space*, *62*, 309–318.
- Narayanan, V. L., S. Gurubaran, and K. Emperumal (2009), Imaging observations of upper mesospheric nightglow emissions from Tirunelveli (8.7°N), *Indian J. Radio Space Phys.*, *38*, 150–158.
- Otsuka, Y., K. Shiokawa, and T. Ogawa (2012), Disappearance of equatorial plasma bubble after interaction with mid-latitude medium-scale traveling ionospheric disturbance, *Geophys. Res. Lett.*, *39*, L14105, doi:10.1029/2012GL052286.
- Paulino, I., H. Takahashi, A. F. Medeiros, C. M. Wrasse, R. A. Buriti, J. H. A. Sobral, and D. Gobbi (2011), Mesospheric gravity waves and ionospheric plasma bubbles observed during the COPEX campaign, *J. Atmos. Sol. Terr. Phys.*, *73*, 1575–1580, doi:10.1016/j.jastp.2010.12.004.
- Prakash, S. (1999), Production of electric field perturbations by gravity wave winds in the E region suitable for initiating equatorial spread F, *J. Geophys. Res.*, *104*(A5), 10,051–10,069, doi:10.1029/1999JA900028.
- Sekar, R., D. Chakrabarty, R. Narayanan, and A. K. Patra (2008), Equatorial Spread F structures and associated airglow intensity variations observed over Gadanki, *Ann. Geophys.*, *26*, 3863–3873.
- Shiokawa, K., Y. Otsuka, and T. Ogawa (2006), Quasiperiodic southward moving waves in 630-nm airglow images in the equatorial thermosphere, *J. Geophys. Res.*, *111*, A06301, doi:10.1029/2005JA011406.
- Shiokawa, K., Y. Otsuka, and T. Ogawa (2009), Propagation characteristics of nighttime mesospheric and thermospheric waves observed by optical mesosphere thermosphere imagers at middle and low latitudes, *Earth Planets Space*, *61*, 479–491.
- Takahashi, H., et al. (2009), Simultaneous observation of ionospheric plasma bubbles and mesospheric gravity waves during the SpreadFEx campaign, *Ann. Geophys.*, *27*, 1477–1487, doi:10.5194/angeo-27-1477-2009.
- Taori, A., and A. Sindhya (2014), Measurements of equatorial plasma depletion velocity using 630 nm airglow imaging over a low latitude Indian station, *J. Geophys. Res. Space Physics*, *119*, 396–401, doi:10.1002/2013JA019465.
- Taori, A., J. J. Makela, and M. Taylor (2010), Mesospheric wave signatures and equatorial plasma bubbles: A case study, *J. Geophys. Res.*, *115*, A06302, doi:10.1029/2009JA015088.
- Taori, A., N. Dashora, K. Raghunath, J. M. Russell III, and M. G. Mlynczak (2011a), Simultaneous mesosphere, thermosphere-ionosphere parameter measurements over Gadanki (13.5°N, 79.2°E): First results, *J. Geophys. Res.*, *116*, A07308, doi:10.1029/2010JA016154.
- Taori, A., A. K. Patra, and L. M. Joshi (2011b), Gravity wave seeding of equatorial plasma bubbles: An investigation with simultaneous F region, E region, and middle atmospheric measurements, *J. Geophys. Res.*, *116*, A05310, doi:10.1029/2010JA016229.
- Taori, A., A. Jayaraman, and V. Kamalakar (2013), Imaging of mesosphere–thermosphere airglow emissions over Gadanki (13.5°N, 79.2°E)—First results, *J. Atmos. Sol. Terr. Phys.*, *93*, 21–28, doi:10.1016/j.jastp.2012.11.007.
- Tsunoda, R. T. (2010), On seeding equatorial spread F: Circular gravity waves, *Geophys. Res. Lett.*, *37*, L10104, doi:10.1029/2010GL043422.
- Tsunoda, R. T., M. Yamamoto, T. Tsugawa, T. L. Hoang, S. Tulasi Ram, S. V. Thampi, H. D. Chau, and T. Nagatsuma (2011), On seeding, large-scale wave structure, equatorial spread F, and scintillations over Vietnam, *Geophys. Res. Lett.*, *38*, L20102, doi:10.1029/2011GL049173.
- Vadas, S. L., and D. C. Fritts (2005), Thermospheric response to gravity waves: Influences of increasing viscosity and thermal diffusivity, *J. Geophys. Res.*, *110*, D15103, doi:10.1029/2004JD005574.
- Valladares, C. E., J. Villalobos, M. A. Hei, R. Sheehan, S. Basu, E. MacKenzie, P. H. Doherty, and V. H. Rios (2009), Simultaneous observation of traveling ionospheric disturbances in the Northern and Southern Hemispheres, *Ann. Geophys.*, *27*, 1501–1508.
- Varney, R. H., M. C. Kelley, and E. Kudeki (2009), Observations of electric fields associated with internal gravity waves, *J. Geophys. Res.*, *114*, A02304, doi:10.1029/2008JA013733.